Rectilinear Coordinate Frames for Deep Sea Navigation

Chris Murphy
Deep Submergence Laboratory
Woods Hole Oceanographic Institution
Woods Hole, MA
Email: cmurphy@whoi.edu

Dr. Hanumant Singh
Deep Submergence Laboratory
Woods Hole Oceanographic Institution
Woods Hole, MA
Email: hanu@whoi.edu

***Abstract*— Since 1964 the National Deep Submergence Facility and Deep Submergence Laboratory at the Woods Hole Oceanographic Institution (WHOI) have performed thousands of scientific dives with human occupied, remotely operated, and towed vehicles. Each of these vehicles uses an equirectangular map projection within their navigation systems, colloquially known as the *AlvinXY* coordinate scheme. Equirectangular projections provide a simple, affine mapping between geographic coordinates and the coordinates of a cartesian grid. Additionally, *AlvinXY* and similar coordinate systems disregard the effect of depth upon the coordinate mapping. Advances in underwater navigational instrumentation during the past forty years now allow localization to such precision that, in some cases, the precision of the navigation solution is comparable to that of errors introduced by working in this simple coordinate space. In this paper, we characterize the effects of projection errors in this system upon vehicle navigation and localization for deep oceanographic vehicles today.**

I. Introduction

The deep sea poses a number of challenges to navigation. Seawater rapidly filters out visible light and makes high frequency radio communications, such as those required by the Global Positioning System, impossible. Between the surface and the seafloor there may be thousands of meters of open ocean to traverse with no fixed reference points. Once the seafloor is reached it may be featureless over large areas. The NDSF operates a fleet of human occupied, remotely operated, autonomous and tethered vehicles out of the Woods Hole Oceanographic Institution (WHOI). Since 1964, these vehicles have granted scientists the ability to explore the deep sea – initially in person, and now via telepresence robotics. Since the early days of the NDSF, these vehicles have shared a common navigation heritage owing to their development in WHOI's Deep Submergence Lab. Each NDSF vehicle, and others at WHOI such as the SeaBED, PUMA and Jaguar Autonomous Underwater Vehicles (AUVs), uses the *AlvinXY* map projection to convert between the latitude and longitude coordinates used on the curved surface of the globe and the rectilinear coordinates of a cartesian grid. This conversion provides two distinct benefits: an improved operator interface, and mathematical simplicity within the AUV navigation code.

First, scientists and engineers often find it easier while planning or reviewing a mission to work in meters on a grid than in degrees on a globe. Deep sea missions are measured in battery kilowatt-hours, hours for human passengers to be subsea or meters of trackline that can be run. *AlvinXY* coordinates provide an easily understandable common reference frame for discussion. Thousands of missions run by the NDSF vehicles over the years have been planned in *AlvinXY* coordinates.

Second, *AlvinXY* coordinates are used as a simplified model of the world for the AUV to navigate within. Acoustic navigation requires trigonometry, which is greatly simplified by working rectilinearly in two dimensions rather than on the surface of the globe. These simplifications allow algorithms to run faster and be debugged easier, valuable attributes for underwater computation. Coordinates can be projected back to latitudes and longitudes afterwards for georeferenced mapping.

While the *AlvinXY* map projection remains suitable for rough planning and visualization purposes, it grows increasingly inappropriate for navigational usage. Advances in acoustic localization, the availability of Doppler Velocity Logs (DVLs) and Fiber-Optic Gyroscopes now allow localization to a much greater precision than was possible in 1964. We disuss two ways these errors manifest themselves – as integration errors within inertial navigation computations (discussed in Section III-A), and as errors in the absolute calculated position from Long Baseline navigation systems (discussed in Section III-B). Finally, I briefly discuss alternatives that may mitigate these errors in Section IV.

II. Background

A. The National Deep Submergence Facility (NDSF)

Over the years, the NDSF vehicles have proved themselves invaluable to fields across the scientific spectrum. A review of the NDSF publication database yields thousands of publications, across fields from archaeology [1], to biology [2], to geochemistry, to vulcanology. First-hand magnetic, gravitational and seismic measurements taken during Project FAMOUS [3], [4] drove our understanding of plate tectonics and other geological processes. The discovery of Tubeworms near the Galapagos in 1977 [5], [6] practically created the field of deep sea vent biology. The Human Occupied Vehicle Alvin has even been used to locate a lost Hydrogen Bomb [7].

Alvin can carry two scientists and a pilot to the seafloor more than four kilometers below the surface. Tethered or remotely operated vehicles like JASON [8] and its successor JASON II [9] now allow scientists to explore the seafloor without the risks or challenges inherent to manned exploration. The ability to switch pilots without vehicle recovery also allows operations around the clock. Most recently, AUVs like the Autonomous Benthic Explorer (ABE) [10], its replacement SENTRY, and the new optically tethered vehicle NEREUS [11], provide a way to explore large areas of the seafloor without any human pilot or supervision. ABE, the grandfather of an entire fleet of AUV's, performed over two hundred dives before being retired this past year.

B. Underwater Navigation

Deep sea vehicles typically incorporate navigation information from a variety of sources. Depth is usually provided independent of horizontal position through measurements of ambient pressure. High accuracy measurement of true heading can be obtained from a Fiber-Optic Gyroscope. While typical surface- or air-based robots might use electromagnetic signaling for horizontal localization (i.e. GPS), seawater rapidly attenuates high frequencies and prevents the use of such technologies. Instead, when underwater geo-referenced navigation is necessary a set of acoustic beacons is typically deployed to form a Long Baseline (LBL) network [12]. These beacons listen for a "ping" at a specific frequency and respond similarly at a different frequency. An AUV interrogates the LBL network by generating a query ping, and measuring how much time elapses before it hears the responses from each beacon. These travel times, together with the known locations of the deployed beacons, provide constraints on the possible locations of the robot.

The low speed of sound through water, around $1500 m/s$, means that position updates are infrequent. Additionally, acoustic communications between the vehicle and the surface may prevent acoustic navigation. To obtain more rapid updates on AUV position, a precision Inertial Navigation System (INS) or a Doppler Velocity Log (DVL) is typically employed as described by Whitcomb et al. in [13]. For those seeking a more detailed background on underwater vehicle navigation, Kinsey et al. recently provided an excellent review of the state of the art [14].

While DVLs are now widely used to provide accurate estimates of velocity when near the seafloor, they have only been in wide use since the 1990's when subsea Digital Signal Processing became practical [15]. Acoustic navigation has been practical for much longer, dating back to at least the 1960's, yet has significantly lower precision. One of the earliest ALVIN expeditions to obtain widespread notice advertised $O(10m - 100m)$ horizontal precision [16]. As such, underwater vehicles were primarily qualitative tools at the time that *AlvinXY* was developed in the 1960's.

C. AlvinXY Map Projection

The *AlvinXY* projection is designed to be easy to understand, and simple to implement. The Y coordinates of an *AlvinXY* projected space are equivalent to meters North of some origin (Northings) and X coordinates are equivalent to meters East of the origin (Eastings). For example, an object located at $(x, y) = (300, 1000)$ in *AlvinXY* space would ideally be found three hundred meters East and one kilometer North of the origin.

```python
import math
def latlon2xy(lat, long, lat0, lon0):
  x = (lon-lon0) * mdeglon(lat0)
  y = (lat-lat0) * mdeglat(lat0)
  return x, y

def xy2latlon(x, y, lat0, lon0):
  lon = x/mdeglon(lat0) + lon0;
  lat = y/mdeglat(lat0) + lat0;
  return lat, lon

def mdeglon(lat0):
  lat0rad = math.radians(lat0)
  return (111415.13 * cos(lat0rad)
          - 94.55 * cos(3.0*lat0rad)
          - 0.12 * cos(5.0*lat0rad) )

def mdeglat(lat0):
  lat0rad = math.radians(lat0)
  return (111132.09 - 566.05 * cos(2.0*lat0rad)
                    + 1.20 * cos(4.0*lat0rad)
                    - 0.002 * cos(6.0*lat0rad) )
```

Fig. 1. Python implementation of `latlon2xy`and `xy2latlon`. The AlvinXY Origin is located at (lat0, lon0).

A typical implementation of the *AlvinXY* projection on a modern computer consists of two main functions, `latlon2xy` and `xy2latlon`. An example Python implementation is given in Listing 1. The algorithm is straightforward; `latlon2xy` calculates the X coordinate by computing the number of degrees longitude that the point is from the origin, and multiplying by a constant scaling factor derived from the origin's latitude. The Y coordinate is similarly calculated from the point's latitude. `xy2latlon` simply performs the inverse operation. The functions are thus an affine transformation between degrees and meters for a given *AlvinXY* projection, based upon the latitude of the origin. Since increasing longitudes correspond strictly to increasing X values, and increasing latitudes strictly to Y values, the map projection can be considered a scaled Equirectangular map projection.

When the *AlvinXY* projection was developed, computers were not available at sea. As a result, the projection equations were developed to be simple and capable of being computed quickly on slide rules and similar equipment. After the initial computation of two scale factors, navigation in *AlvinXY* consists only of simple multiplication and addition. Computation of these initial scale factors represents most of the complexity of the projection equations.

In Listing 1, the scale factors are calculated in the `mdeglat` and `mdeglon` subroutines. These functions compute the length of one degree latitude or longitude for a given latitude on the globe. They were derived by George B. McClellan Zerr in 1901 for *The American Mathematical Monthly* [17]. Zerr explained that the equations shown below yield the length of one degree longitude (l) and latitude (L) at a given latitude (θ), for a given major axis length (a) and eccentricity (e) of the Earth.

$$l = \frac{\pi a(1-e^2)}{180(1-e^2\sin^2\theta)^{\frac{3}{2}}}$$
$$L = \frac{\pi a\cos\theta}{180\sqrt{1-e^2\sin^2\theta}}$$

An arbitrarily close approximation to these equations can then be obtained using Newton's generalized binomial theorem as shown below, where N is the desired number of terms in the expanded result.

$$l = \frac{\pi a\cos\theta}{180}\sum_{k=0}^{N-1}\left[\frac{e^{2k}\sin^{2k}\theta}{k!}\prod_{n=0}^{k-1}\left(-\frac{1}{2}+k-n\right)\right]$$
$$L = \frac{\pi a(1-e^2)}{180}\sum_{k=0}^{N-1}\left[\frac{e^{2k}\sin^{2k}\theta}{k!}\prod_{n=0}^{k-1}\left(\frac{1}{2}+k-n\right)\right]$$

When approximated to the number of terms typically used for the *AlvinXY* equations, with a and e set to the major axis length and eccentricity of the Clarke 1866 Spheroid, the equations in Listing 1 result.

III. Analysis

Unfortunately, the simplicity of the *AlvinXY* projection comes at a cost. The example above of an object located at $(x, y) = (300, 1000)$ on an *AlvinXY* grid ignores the fact that if you start at one point on the Earth, go North 1000 meters and then East 300 meters, you will arrive in a different location than if you first go East 300 meters and then North 1000 meters. There are a number of navigation errors introduced by the *AlvinXY* projection, due to differences between the model of the earth assumed by the projection, a plane, and the actual surface of the globe. To understand the nature of the errors more carefully, it helps to consider some of the specific ways in which the *AlvinXY* model approximates reality. While the three factors discussed below are treated independently, they all reflect different aspects of inaccurate modelling of the Earth's true form.

Rectilinearity of Meridians and Parallels – To obtain a simple mapping between lines of latitude and longitude and the Cartesian plane, a constant scaling factor is used between degrees of latitude and meters. A second constant scaling factor is used between degrees of longitude and meters. In reality, the length of one degree of longitude varies from over 100000 meters at the equator to zero meters at the poles.

Approximation of the Earth's Shape – A numerical model of the globe is employed to calculate the scaling factors referenced above. These scale factors are chosen to fit the model at the location of the *AlvinXY* origin – conversely, the scale factor is correct *only* when located exactly at the origin. The model of the earth typically used by cartographers is a spheroid, also known as a biaxial ellipsoid. While the *AlvinXY* projection equations are based upon a spheroidal model, the model they use is antiquated and inaccurate.

Ignoring Depth – *AlvinXY* derives the scale factors from the surface of the spheroidal model, the radius of which is approximately 6400 kilometers (see Table I). NDSF vehicles can easily dive to a few kilometers depth, with one (Nereus) able to withstand the pressure of full ocean depths at 11 kilometers. The scaling between degrees on the surface is not identical to the scaling for the (non-spheroidal) shape eleven kilometers deeper.

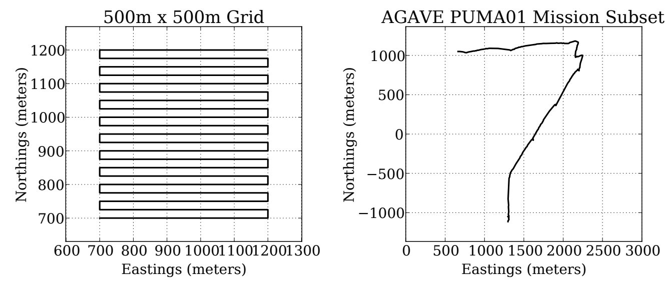

Fig. 2. Vehicle track for the test missions used within this paper.

Throughout this section, two different missions will be used to evaluate the effects of each aspect of the *AlvinXY* projection. The first mission is a grid consisting of 21 tracklines, traveling East at first and gradually working across a $500m \times 500m$ survey grid from South to North. The grid begins at $(x, y) = (700, 700)$, approximately 1 kilometer North-East (arbitrarily) of the *AlvinXY* origin. This mission is simulated at latitudes spanning the globe. The second mission is a subset of an actual mission, PUMA01, performed by a SeaBED AUV [18] during the Arctic Gakkel Vents Expedition [19]–[22]. The *AlvinXY* origin for PUMA01 was located at $85°38'$N, well north of the Arctic circle. This example was selected to provide a real world example of the effects when they are at their most apparent. The vehicle track for the both missions is shown in Figure 2, with the vehicle starting at the Southern end and working North. The total length of the trackline used is between 4 and 4.5 kilometers.

A. Doppler Velocity Log (DVL) and Inertial Navigation

Doppler Velocity Logs (DVLs) provide seafloor-relative velocity estimates for underwater vehicles by measuring the doppler shift of pulses sent out by an array of sonar transducers. A thorough review of DVL based navigation for underwater vehicles is available in [23]. When within range of the bottom, also known as being in "bottom-lock" mode, DVLs are capable of remarkable precision. Whitcomb et al. report precisions of 0.3% of reported body velocity while using a Doppler Velocity Log in bottom-lock mode [14]. McEwen et al. report incredible precision as high as 0.05% of the distance travelled by their AUV [24].

Whether a high precision DVL or some other source of precise vehicle velocities is used, measurements are typically numerically integrated to provide updated vehicle locations. Each of the approximations made by the *AlvinXY* projection has an effect upon the results of this integration, which is described in turn below. The results in each case consider only the error resulting from the specific approximation being discussed, to facilitate relative comparison.

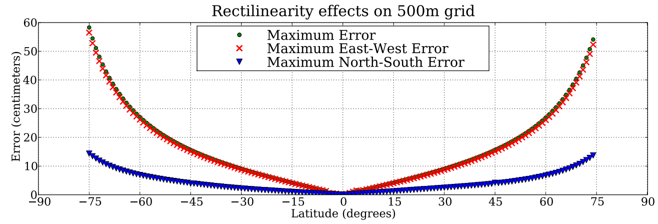

Fig. 3. Maximum difference between locations calculated using the `latlon2xy` equations and locations calculated using the Vincenty method over a $500m \times 500m$ grid at various latitudes.

1) Rectilinearity: As mentioned above, the AlvinXY projection assumes that meridians and parallels are perpendicular within the mapped area. In reality, the length of one degree longitude varies a measureable amount over even a moderately sized survey site. To quantify the effects of this approximation, the $500m$ grid mission was simulated at latitudes spanning the globe. The calculated location using the *AlvinXY* map projection was compared to the location calculated using the Vincenty direct method. The Vincenty direct method [25], along with the Bowring [26] method and others, provide a arbitrarily precise method for determining a destination based upon an original location, and travelled distance and bearing on the surface of a spheroid. For both the *AlvinXY* projection equations and the Vincenty method, the Clarke 1866 spheroid was used. Figure 3 shows the distance between the destination calculated in *AlvinXY* space, and the distance resulting from the Vincenty method of integration on the spheroid.

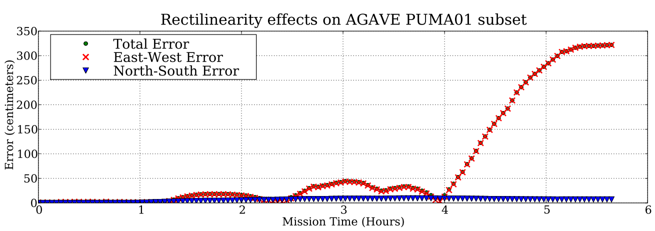

Fig. 4. Difference between locations calculated using the `latlon2xy` equations and locations calculated using the Vincenty method during the AGAVE PUMA01 mission over time.

The difference between the two methods ranges from five to upwards of twenty centimeters at moderate latitudes. The error is at a maximum, unsurprisingly, near the poles. The data for the PUMA01 mission was originally recorded in AlvinXY coordinates. Analysis of the PUMA01 mission shows that the rectilinearity assumptions imposed by navigating in *AlvinXY* account for a few meters of error over the course of this dive subset.

2) Spheroidal Models of the Earth: All map projections must use a model to determine the relationship between angular measures and linear distances on the surface of the earth. While the earliest such models assumed the earth to be spherical, modern cartography defines latitudes and longitudes relative to a reference spheroid; a biaxial ellipsoid of a defined size, slightly flattened at the poles. The AlvinXY Coordinate scheme uses the "Clarke 1866" reference spheroid for transformations anywhere on the globe – so named because the model was developed in 1866 by Alexander Ross Clarke.

Within the United States, the dominant mapping datum (or system), was the North American Datum of 1927 (NAD27) until the 1980's. NAD27 used the same 1866 Clarke spheroid as the AlvinXY coordinate scheme, but made the key alteration of offsetting it from the center of the earth. This minimized the model error within the continental United States, but increased the error elsewhere on the globe. As the use of satellite geodesy overtook land-based observation, it became clear that the spheroidal model derived by Clarke was not a precise enough model for the positioning accuracy of modern technology.

Spheroid	Major Axis (m)	Eccentricity
Clarke 1866	6378206.4	0.0822718542230
Clarke 1878	6378190	0.0824832600347
GRS80	6378137.0	0.0818191910435
WGS84	6378137.0	0.0818191909289

TABLE I
MAJOR AXIS AND ECCENTRICITY OF SELECTED SPHEROIDS.

In 1983, the North American Datum was revised to use a new spheroidal model for the earth, GRS80, which is seventy meters larger at the equator than the Clarke spheroid. The desire to have a single globally accurate model led to the development of the World Geodetic System in 1984 (WGS84), and resulted in a minor revision of the eccentricity in the ninth decimal place. The final WGS84 spheroid is geocentric, and usable across the globe. The WGS84 or GRS80 model is now used in almost all GPS receivers and on most navigational charts. It is also a significantly more accurate model of the earth, which results in better accuracy of measured distances along the surface. The Clarke 1866 spheroid has not been recommended for worldwide mapping use for a number of years.

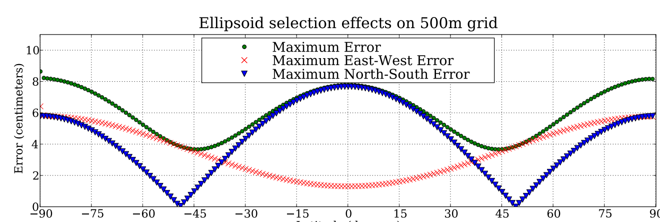

Fig. 5. Maximum difference between locations calculated using the `latlon2xy` equations with the Clarke 1866 reference spheroid and those calculated using the WGS84 spheroid over a $500m \times 500m$ grid at various latitudes.

The grid mission was again simulated at latitudes spanning the globe, first with the Clarke 1866 reference spheroid and then with the WGS84 reference spheroid. The basic *AlvinXY* equations were used in both cases. The difference between the two methods ranges between 15 and 35 centimeters, depending on the latitude. It is at maximum near the poles, though interestingly remains high at the equator. The minimum error is found at $45°$ latitude in both hemispheres.

The data for the PUMA01 mission was originally recorded in AlvinXY coordinates. Analysis of the PUMA01 mission shows that the choice of the Clarke 1866 spheroid resulted in an error of between six and twelve centimeters for the selected mission segment.

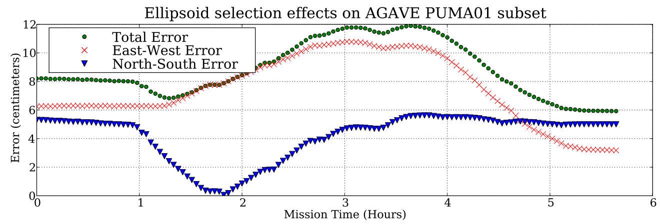

Fig. 6. Difference between locations calculated using the `latlon2xy` equations with the Clarke 1866 reference spheroid and those calculated using the WGS84 spheroid during the AGAVE PUMA01 mission over time.

3) Depth Effects: Underwater vehicles routinely work thousands of meters below the surface of the sea. Map projections, typically designed for the earth's surface, do not accurately represent scales at these depths. To approximate the effects of ignoring this depth offset, locations using the *AlvinXY* coordinate scheme were compared using the Clarke 1866 spheroid, and an spheroid kilometers smaller in its major and minor axes. For the grid dive, the error was approximately 75m east to west, and 75m north to south. The effects of this difference in size on the PUMA01 dive are shown in Figure and 7.

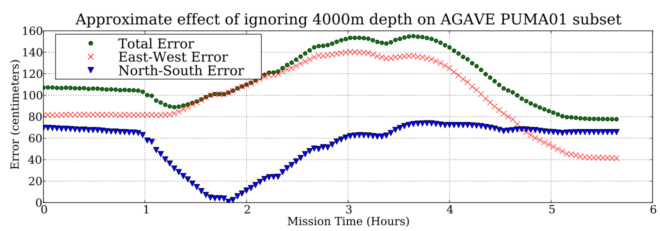

Fig. 7. Approximate dfference between locations calculated using the `latlon2xy` equations corrected for depth and the uncorrected versions during the AGAVE PUMA01 mission.

The errors due to ignoring depth in this approximation are uniformly large across latitudes. However, a height offset from the surface of a spheroid does not just alter the size, but the shape as well. A surface offset from a spheroid by a constant height h can be described by the parametric equations shown below [27].

$$\begin{bmatrix} X \\ Y \\ Z \end{bmatrix} = \begin{bmatrix} [\frac{\rho_e}{\sqrt{1-e^2\sin^2\phi}} + h]\cos\phi\cos\lambda \\ [\frac{\rho_e}{\sqrt{1-e^2\sin^2\phi}} + h]\cos\phi\sin\lambda \\ [\frac{\rho_e}{\sqrt{1-e^2\sin^2\phi}}(1-e^2) + h]\sin\phi \end{bmatrix}$$

Methods for navigating that fully account for this change in size and shape, and account for non-rectilinearity are proposed in Section IV. In addition to accounting for depth below sea level, it worth acknowledging that the earth is not a perfect spheroid; mean sea level varies from the idealized WGS84 spheroid by up to a hundred meters, as shown in Figure 8. Tidal influences also add time-varying factors to the transformation between sea depth and offset from the reference spheroid.

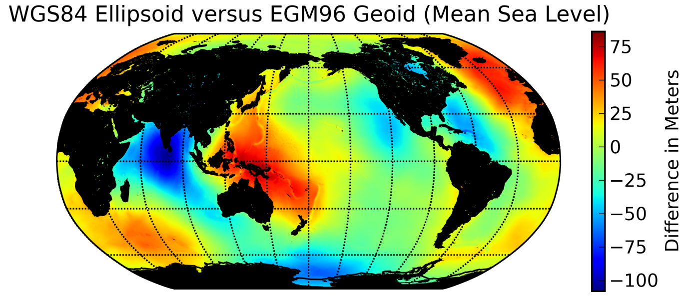

Fig. 8. Difference in meters between the WGS84 spheroid and the approximate mean sea level, as modeled by the EGM96 Geoid [28].

B. Long Baseline (LBL) Navigation

Long Baseline (LBL) acoustic positioning depends upon a previously established network of acoustic beacons. These beacons are typically moored to the seafloor with tethers, and their locations have been carefully determined during an initial site survey. During operation, the vehicle typically interrogates the beacons acoustically and measures the round-trip travel-time to each beacon. Travel times are converted to slant ranges, which yield spherical constraints on vehicle position and can be used to trilaterate the vehicle location in two or three dimensions [29]. Jakuba et al. describe a number of possible modifications to the traditional spherical LBL model [30].

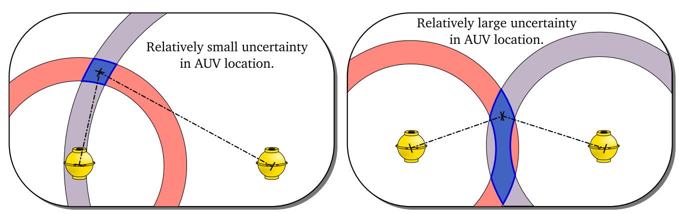

Fig. 9. LBL uncertainty is inherently higher near the LBL baseline due to the geometry of intersection. Any uncertainty in range measurements result in a much larger location uncertainty near the baseline.

The precision of modern LBL navigation depends on a number of factors, including the depth of the transponders, latitude of operation, and operating frequency. The positioning precision of LBL is inherently lower near the LBL baseline due to the geometry, meaning that any errors will be magnified there as shown in Figure 9. Whitcomb reported $O(0.1m)$ LBL precision with JASON operating at a depth of five hundred meters, with higher precision after the incorporation of Doppler Velocity Log measurements [13]. Bingham further characterized LBL positioning uncertainty as $O(0.1m - 1m)$ for a two kilometer baseline [31].

Error in an LBL solution can come from two distinct sources. First, there may be error in the calculated slant range due to inaccurate measurement of sound speed, or more complex acoustic effects. Second, error may arise when slant ranges are transformed into a position. Underwater vehicles are often equipped with pressure sensors capable of providing a precise depth measurement. Thus, when calculating a vehicle position from acoustic slant ranges, it is common to 'collapse' the three-dimensional spherical problem to a two-dimensional problem of circular intersection at the depth of the vehicle. For

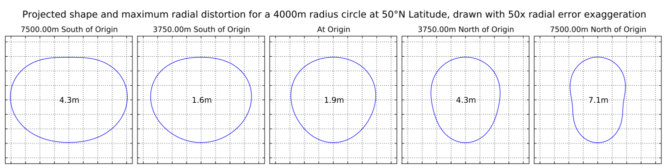

Fig. 10. Projected shape of a circle in *AlvinXY* coordinates, with the deviation from circular magnified fifty times to increase visibility.

vehicles using the *AlvinXY* map projection, solving the two-dimensional problem in *AlvinXY* coordinates seems logical. Unfortunately, solving in *AlvinXY* has the effect of essentially introducing error into range measurements, as a constant radius circle on the surface of the globe does not project to a circle in the *AlvinXY* coordinate plane. Figure 10 shows the distortion for a circle of constant radius at $50°N$ Latitude.

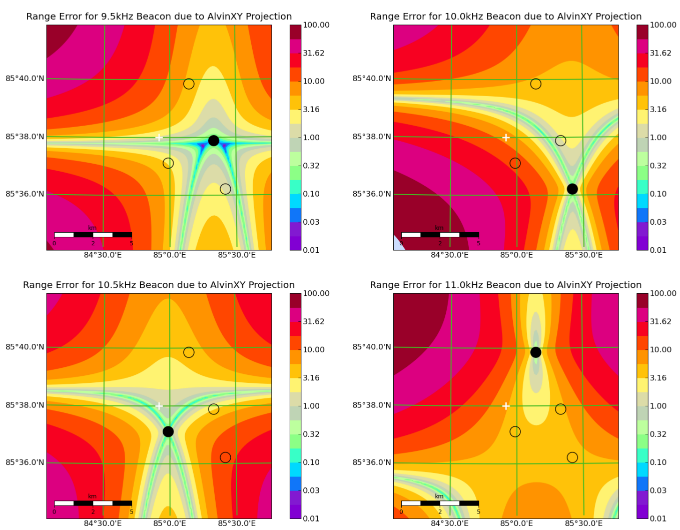

Fig. 11. Error in calculated range to LBL beacons due to working in *AlvinXY* coordinates.

As a specific example, the difference between the *AlvinXY* calculated range to each long baseline transponder during the AGAVE expedition and the actual range is shown in Figure 11. Each beacon was at a depth of approximately four kilometers. To calculate the actual range to each location, beacon locations were transformed into an earth-centered earth-fixed (ECEF) XYZ coordinate frame, and the linear distance to a vehicle at the same depth as the transponder was calculated. The ECEF coordinate frame typically designates Z as passing through the North Pole, and X and Y as being perpendicular to each other passing through the center of the Earth's mass. This coordinate scheme is supported by numerous software libraries, and used in GPS units and many other applications. While solving in ECEF as described remains an approximation, the minimal curvature of the earth over ten kilometers results in roughly a millimeter of difference from the actual distance.

The difference between the ranges calculated in *AlvinXY* and those calculated in ECEF coordinates is significant – on the order of a few meters. This is the same order of magnitude as LBL's precision and accuracy, if not higher.

For any pair of these four transponders, a location can be calculated. The error in range calculations results in error in the location estimate. This location error for each pair of beacons is shown in Figure 12. The vehicle was assumed to be at a depth half-way between each transponder, and a spherical solution was calculated from the two slant ranges spheres in the ECEF coordinate frame. These calculation

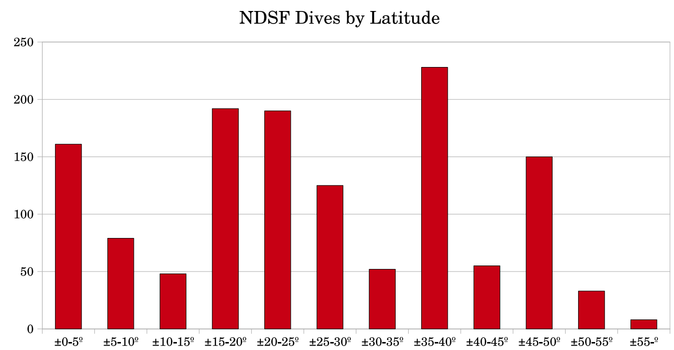

Fig. 13. Number of NDSF dives by latitude.

errors are not limited to polar latitudes. Figure 13 shows a histogram of NDSF dive locations over the past several years; numerous dives have occurred at latitudes up to $55°$ on the Juan de Fuca ridge. The set of plots in Figure 14 shows the calculated location error for a long baseline network located at the latitude of the Juan de Fuca ridge. In each of the plots, the *AlvinXY* origin is located at a different orientation to the baseline to show the wide (and unintuitive) range of error surfaces that can result.

IV. Alternatives

For much of *AlvinXY* 's history it has been used as a catch-all tool for navigation and mapping. As navigation accuracy and precision continue to improve, a similar catch-all solution may be difficult to find. Map projections all trade off navigation, path planning, estimation, and operational benefits. A number of map projections may be found to have better performance with similar complexity. The widespread adoption of Universal Transverse Mercator (UTM) makes it appealing, but UTM averages error across six degrees of longitude. For survey sites of a few kilometers, this introduces unnecessary error. A local Transverse Mercator projection on the other hand can have relatively low error across a large survey area, but

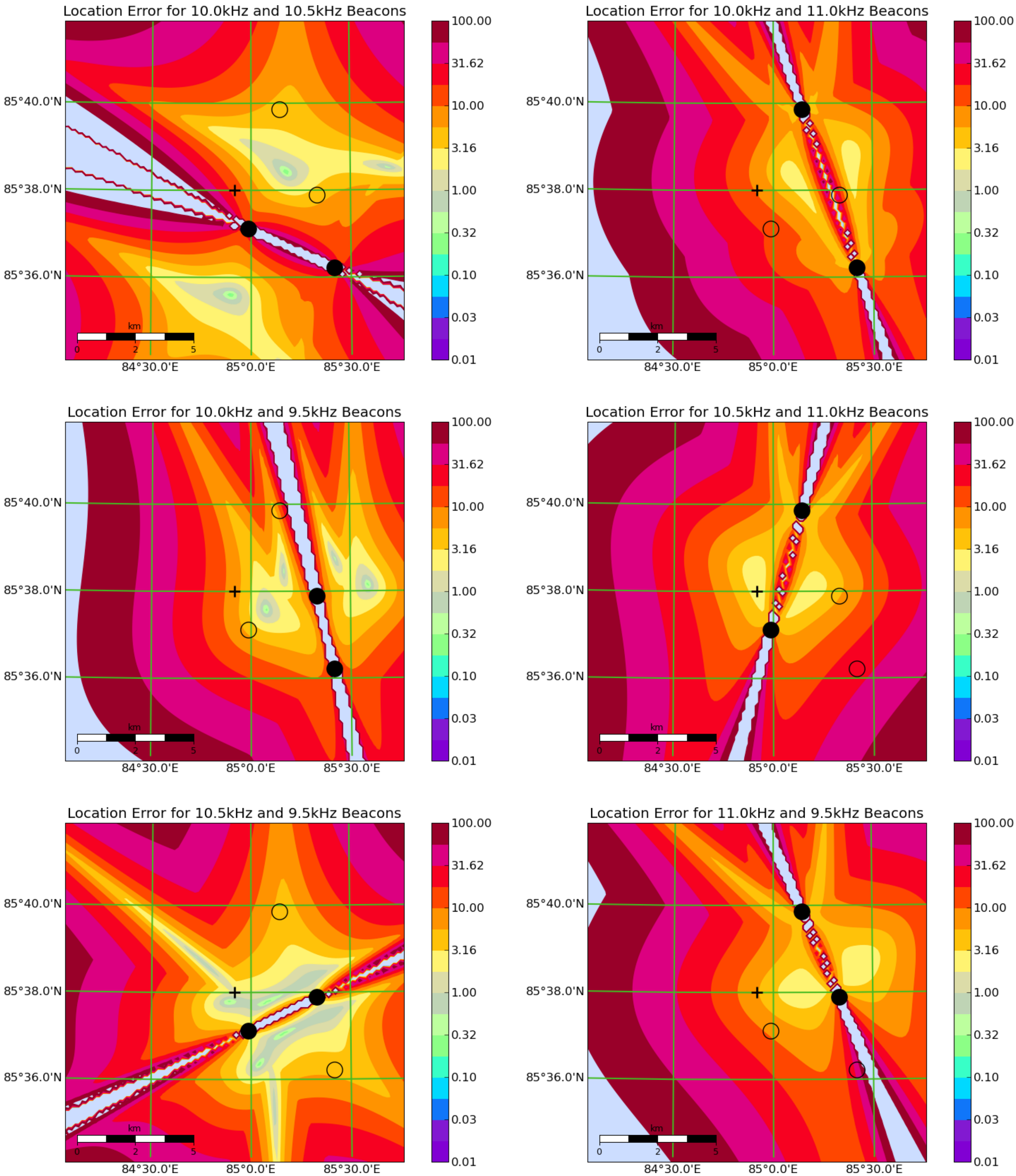

Fig. 12. Error in calculated vehicle location due to working in *AlvinXY* coordinates.

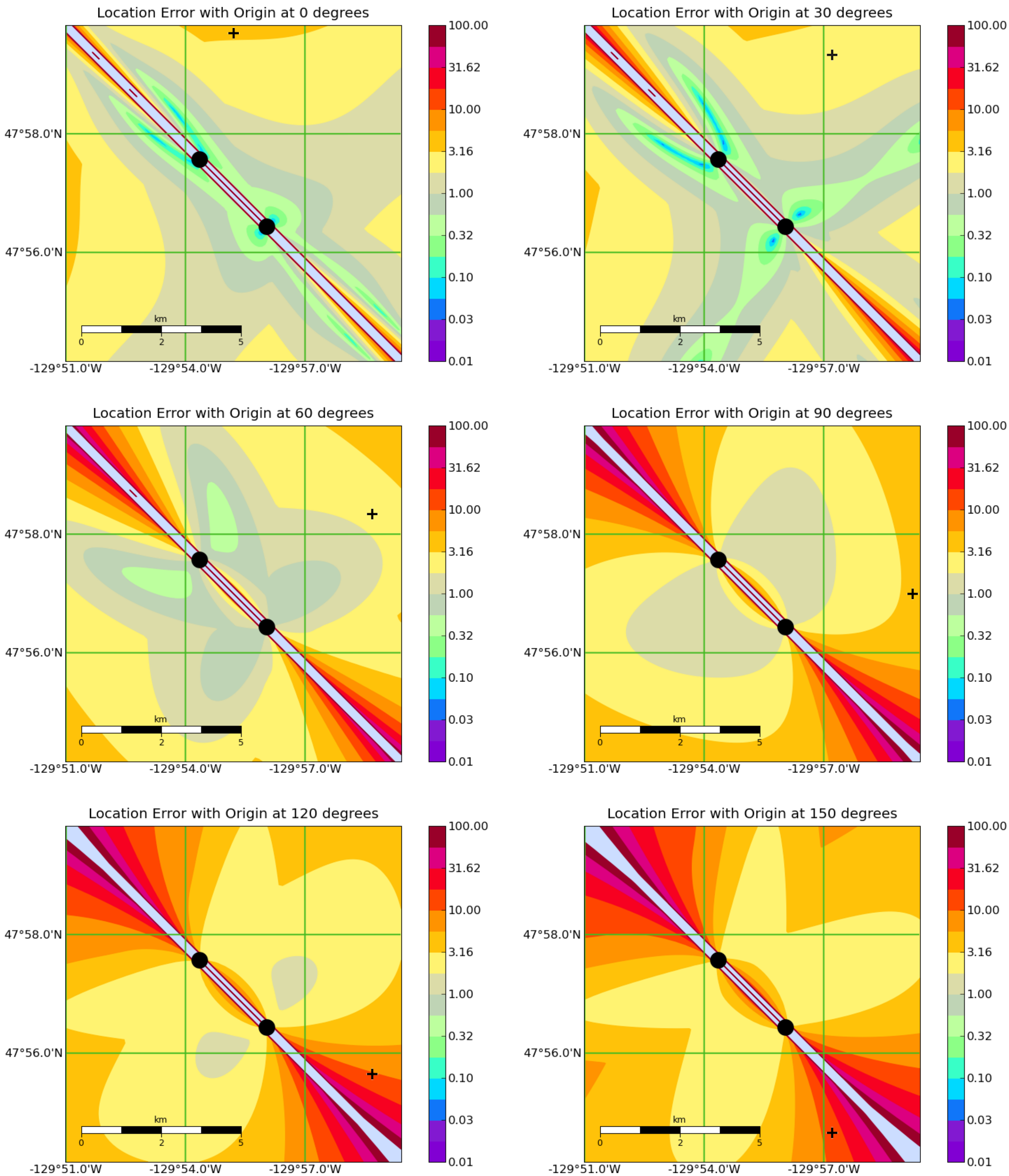

Fig. 14. Location error at 45° North for a long baseline network with a variety of origin geometries. The LBL baseline is three kilometers long, and the origin is located five kilometers from the center of the baseline in each case.

still requires that depth be taken into consideration. Yet another option is to select a locally appropriate map projection for each research expedition, as surveyors assign map projections to regions.

Alternatively, Moore et al. describe a novel navigation method they employed successfully for the Darpa Grand Challenge, relying upon a smoothly (and constantly) updating local reference frame [32]. While their implementation relied upon a specific map projection, a similar method could be employed using a Local Tangent Plane. A Local Tangent Plane, in this

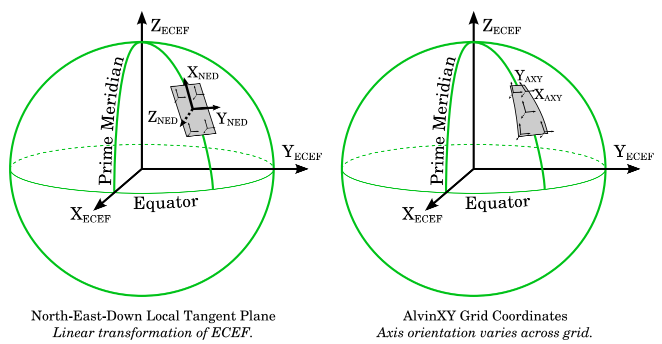

Fig. 15. A comparison of "North-East-Down" local tangent plane coordinates and the *AlvinXY* coordinate grid.

case a North-East-Down (NED) reference frame, is compared in Figure 15 to the *AlvinXY* projection. The NED reference frame offers many of the benefits of *AlvinXY* ; East and North are intuitively along the axes at the origin. Unlike the *AlvinXY* projection however, NED coordinates (represented as x_N, y_N, and z_N below) use a flat reference plane in three dimensions rather than projecting the curved earth surface into two dimensions. Integration over short distances, like those measured by a DVL, can be quite accurate if a new NED reference frame is used at each time step.

$$\begin{bmatrix} x_N \\ y_N \\ z_N \end{bmatrix} = \begin{bmatrix} \cos\lambda & -\sin\lambda & 0 \\ -\sin\phi\sin\lambda & -\sin\phi\cos\lambda & -\cos\phi \\ \cos\phi\sin\lambda & \cos\phi\cos\lambda & -\sin\phi \end{bmatrix} \begin{bmatrix} x_E - x_0 \\ y_E - y_0 \\ z_E - z_0 \end{bmatrix}$$

The North-East-Down coordinate frame is simply a rigid transformation (above) of the ECEF coordinates discussed previously. It, or ECEF, also provides a useful coordinate scheme for long baseline networks. Latitude, longitude and height measurements can readily be converted to XYZ using tools like PROJ.4 [33], [34]. Long baseline localization can then be performed by determining the three-dimensional ring of intersection for two range spheres (or range surfaces generated through acoustic raytracing), and the intersection of that ring with the vehicle's depth.

V. Conclusions

The effects of the *AlvinXY* approximations are largely less than one percent of the measured quantities, in some cases significantly less. Yet given the evolution of deep sea navigation and mapping technology, these error levels approach those that should be considered significant. With computers now widely available while at sea the underlying simplicity of an equirectangular projection no longer remains a compelling reason to use it. Given the long history of the *AlvinXY* projection, some applications may suggest continued use of the projection to maintain compatibility with previously collected datasets. Where it continues to be used, LBL inaccuracies will result in incorrect location matching across the surface / ocean boundary, and LBL fixes will be dependent upon the specific LBL beacons and LBL beacon locations used.

While this paper focuses on the cost to accuracy imposed by the *AlvinXY* projection there are other, perhaps equally important, concerns posed by its usage. The details of the projection are largely obscured by binomial approximation, which leaves the underlying assumptions difficult to determine without documentation. In Zerr's day this approximation was a necessary step; division, exponentiation and square roots were tedious and time consuming. Trigonometric identities, like $\sin^2\theta = \frac{1-\cos 2\theta}{2}$, allowed the final result to consist of only simple multiplications and cosine table lookups. To a modern computer, these computational simplifications hold significantly less importance. By clouding the equations through a binomial expansion the true methods of the *AlvinXY* transformation are difficult to deduce and understand. It is extremely difficult, for instance, to determine which reference spheroid the transformation uses without rederiving the full binomial expansion for a variety of spheroids. Given the now pervasive usage of these transformations, this is not a consequence to be ignored.

Second, the *AlvinXY* projection is only used within the Deep Submergence Lab and National Deep Submergence Facility. As DSL and the NDSF's primary goals and skills are well removed from map projection development, a solution like *AlvinXY* is likely to be adopted as reasonable rather than attempting to delve into the complex world of cartography. Additionally, the use of a custom projection means that *AlvinXY* coordinates are unsupported by existing map projection tools and libraries. Since the Equirectangular projection has few modern practical uses, it is typically used with a simple spherical model of the earth, and therefore the specifics of *AlvinXY* are not supported[1].

While this paper has focused on the specifics of the AlvinXY projection, the use of a "local Cartesian XY" coordinate frame is widespread within field robotics, as it greatly simplifies the mathematics of navigation and localization. Unfortunately, the details of map projections seem to not always be well understood – a brief survey of open source robotics software platforms suggests that a large number of adhoc solutions exist in the field. Thus, a number of these lessons may be more broadly applicable to the robotics community

[1]For instance, attempting to configure PROJ.4 [33] for an *AlvinXY* origin of $4^\circ N, 23^\circ E$ with a configuration like `+proj=eqc +lat_ts=4 +lat_0=4 +lon_0=23 +ellps=clrk66` will appear to work, but PROJ.4 will instead use a spherical model with a radius of the major axis for the specified spheroid. In addition, PROJ.4 will ignore the lat_0 parameter for the Equirectangular projection.

at large. For the reader whose interest in map projections has been piqued, Snyder [35] still offers one of the most accessible introductions to the topic, and includes descriptions of a large number of map projections. His book can be found for free on the USGS website, and is linked from the bibliography.

REFERENCES

[1] R. D. Ballard, L. E. Stager, D. Master, D. Yoerger, D. Mindell, L. L. Whitcomb, H. Singh, and D. Piechota, "Iron age shipwrecks in deep water off ashkelon, israel," *American Journal of Archaeology*, vol. 106, no. 2, pp. 151–168, Apr. 2002.

[2] D. S. Kelley, J. A. Karson, G. L. Früh-Green, D. R. Yoerger, T. M. Shank, D. A. Butterfield, J. M. Hayes, M. O. Schrenk, E. J. Olson, G. Proskurowski, M. Jakuba, A. Bradley, B. Larson, K. Ludwig, D. Glickson, K. Buckman, A. S. Bradley, W. J. Brazelton, K. Roe, M. J. Elend, A. Delacour, S. M. Bernasconi, M. D. Lilley, J. A. Baross, R. E. Summons, and S. P. Sylva, "A serpentinite-hosted ecosystem: The lost city hydrothermal field," *Science*, vol. 307, no. 5714, pp. 1428–1434, Mar. 2005.

[3] R. D. Ballard and T. H. V. Andel, "Project FAMOUS: Operational techniques and American submersible operations," *Geological Society of America Bulletin*, vol. 88, no. 4, pp. 495–506, Apr. 1977.

[4] K. C. Macdonald, "Exploring the global mid-ocean ridge: A quarter-century of discovery," *Oceanus*, Mar. 1998.

[5] R. D. B. J. B. Corliss, "Oases of life in the cold abyss," *National Geographic Magazine*, no. 152, pp. 441–453, Oct. 1977.

[6] J. B. Corliss, J. Dymond, L. I. Gordon, J. M. Edmond, R. P. von Herzen, R. D. Ballard, K. Green, D. Williams, A. Bainbridge, K. Crane, and T. H. van Andel, "Submarine thermal springs on the galápagos rift," *Science*, vol. 203, no. 4385, pp. 1073–1083, Mar. 1979.

[7] B. Moran, "The day they lost the H-Bomb – and how they got it back," *Invention & Technology*, vol. 20, no. 2, Fall 2004.

[8] R. D. Ballard, D. R. Yoerger, W. K. Stewart, and A. Bowen, "ARGO/JASON: a remotely operated survey and sampling system for full-ocean depth," in *OCEANS, 1991. Proceedings of MTS/IEEE*, 1991, pp. 71–75.

[9] B. Elder, A. Bowen, M. Heintz, M. Naiman, C. Taylor, W. Seller, J. Howland, and L. Whitcomb, "Jason 2: a review of capabilities," in *Eos Trans. AGU Fall Supplement*, 2003, abstract.

[10] D. R. Yoerger, M. V. Jakuba, A. M. Bradley, and B. Bingham, "Techniques for deep sea near bottom survey using an autonomous vehicle," *International Journal of Robotics Research*, vol. 26, no. 1, pp. 41–54, 2007.

[11] A. Bowen, D. Yoerger, L. Whitcomb, and D. Fornari, "Exploring the deepest depths: Preliminary design of a novel light-tethered hybrid ROV for global science in extreme enviornments," *Marine Technology Society Journal*, no. 2, pp. 92–101, 38 2004.

[12] P. H. Milne, *Underwater Acoustic Positioning Systems*. Houston: Gulf Publishing Company, 1983.

[13] L. L. Whitcomb, D. R. Yoerger, H. Singh, and J. Howland, "Advances in underwater robot vehicles for deep ocean exploration: Navigation, control, and survey operations," in *Robotics Research - The Ninth International Symposium*. London: Springer-Verlag Publications, 2000, pp. 439–448.

[14] J. C. Kinsey, R. M. Eustice, and L. L. Whitcomb, "A survey of underwater vehicle navigation: Recent advances and new challenges," in *IFAC Conference of Manoeuvering and Control of Marine Craft*, Lisbon, Portugal, September 2006, invited paper.

[15] K. V. Jorgensen, B. L. Grose, and F. A. Crandall, "Doppler sonar applied to precision underwater navigation," in *IEEE/MTS OCEANS*, vol. 2, Victoria, BC, Canada, Oct. 1993, pp. 469–474.

[16] J. Jarry and A. Farcy, "Navigation system used by submersibles in FAMOUS project," in *IEEE/MTS OCEANS*, vol. 7, sep 1975, pp. 882–886.

[17] G. B. M. Zerr, "The length of a degree of latitude and longitude for any place," *The American Mathematical Monthly*, vol. 8, no. 3, pp. 60–61, Mar. 1901.

[18] H. Singh, A. Can, R. Eustice, S. Lerner, N. McPhee, O. Pizarro, and C. Roman, "Seabed AUV offers new platform for high-resolution imaging," *EOS, Transactions of the AGU*, vol. 85, no. 31, pp. 289,294–295, Aug. 2004.

[19] C. Kunz, C. Murphy, H. Singh, C. Willis, R. A. S. nd Sandipa Singh, T. Sato, K. Nakamura, M. Jakuba, R. Eustice, R. Camilli, and J. Bailey, "Toward extraplanetary under-ice exploration: Robotic steps in the arctic," *Journal of Field Robotics Special Issue on Space Robotics*, vol. 26, no. 4, 2009.

[20] C. Kunz, C. Murphy, R. Camilli, H. Singh, J. Bailey, R. Eustice, C. Roman, M. Jakuba, C. Willis, T. Sato, K. ichi Nakamura, and R. A. Sohn, "Deep sea underwater robotic exploration in the ice-covered Arctic ocean with AUVs," in *Proc. IEEE/RSJ Int. Conference on Intelligent Robots and Systems*, Nice, France, Sept. 2008.

[21] R. Sohn, C. Willis, S. Humphris, T. Shank, H. Singh, H. Edmonds, C. Kunz, U. Hedman, E. Helmke, M. Jakuba, B. Liljebladh, J. Linder, C. Murphy, K. Nakamura, T. Sato, V. Schlindwein, C. Stranne, M. Tausenfreund, L. Upchurch, P. Winsor, M. Jakosson, and A. Soule, "Explosive volcanism on the ultraslow-spreading Gakkel ridge, Arctic Ocean," *Nature*, vol. 453, no. 7199, pp. 1236–1238, June 2008.

[22] R. A. Sohn, H. Edmonds, S. Humphris, T. Shank, H. Singh, B. Ericsson, U. Hedman, M. Jakuba, C. Kunz, B. Larsson, B. Liljebladh, J. Linder, C. Murphy, K. Nakamura, C. Pontbriand, T. Sato, V. Schlindwein, C. Strane, M. Tausendfreund, L. Upchurch, C. Willis, and P. Winsor, "Scientific scope and summary of the Arctic Gakkel vents (AGAVE) expedition," in *EOS, Transactions of the AGU*, vol. 88, 2007.

[23] L. L. Whitcomb, D. R. Yoerger, and H. Singh, "Advances in doppler-based navigation of underwater robotic vehicles," in *IEEE International Conference on Robotics and Automation*, vol. 1, Detroit, MI, 1999, pp. 399–406.

[24] R. McEwen, H. Thomas, D. Weber, and F. Psota, "Performance of an AUV navigation system at arctic latitudes," in *IEEE/MTS OCEANS*, 2003.

[25] T. Vincenty, "Direct and inverse solutions of geodesics on the ellipsoid with application of nested equations," *Survey Review*, vol. 22, no. 176, pp. 88–93, Apr. 1975.

[26] B. R. Bowring, "The direct and inverse problems for short geodesic lines on the ellipsoid," *Surveying and Mapping*, vol. 41, no. 2, pp. 135–141, 1981.

[27] R. J. Mathar, "Geodetic line at constant altitude above the ellipsoid," arXiv PrePrint, 2007, available from http://arxiv.org/abs/0711.0642v3.

[28] F. G. Lemoine, D. E. Smith, L. Kunz, R. Smith, E. C. Pavlis, N. K. Pavlis, S. M. Klosko, D. S. Chinn, M. H. Torrence, R. G. Williamson, C. M. Cox, K. E. Rachlin, Y. M. Wang, S. C. Kenyon, R. Salman, R. Trimmer, R. H. Rapp, and R. S. Nerem, "The development of the NASA GSFC and NIMA joint geopotential model," in *Gravity, Geoid and Marine Geodesy*, J. Segawa, H. Fujimoto, and S. Okubo, Eds., vol. 117. International Association of Geodesy Symposia, 1997, pp. 461–469.

[29] M. M. Hunt, W. M. Marquet, D. A. Moller, K. R. Peal, W. K. Smith, and R. C. Spindell, "An acoustic navigation system," Woods Hole Oceanographic Institution, Woods Hole, Massachusetts 02543 USA, Tech. Rep. WHOI-74-6, Dec. 1974.

[30] M. Jakuba, C. Roman, H. Singh, C. Murphy, C. Kunz, C. Willis, T. Sato, and R. Sohn, "Field report: Long-baseline acoustic navigation for under-ice AUV operations," *J. Field Robotics*, vol. 25, no. 8, July 2008.

[31] B. S. Bingham, "Precision autonomous underwater navigation," Ph.D. dissertation, Massachusetts Institute of Technology, Cambridge, MA, May 2003.

[32] D. Moore, A. S. Huang, M. Walter, E. Olson, L. Fletcher, J. Leonard, and S. Teller, "Simultaneous local and global state estimation for robotic navigation," in *Proceedings of the 2009 IEEE International Conference on Robotics and Automation*, Kobe, Japan, May 2009, to appear.

[33] G. Evenden, "Proj.4 - cartographic projections library," 2000, available from http://trac.osgeo.org/proj/.

[34] H.-G. Wenzel, "Hochauflösende kugelfunktionsmodelle für das gravitationspotential der erde," *Wissenschaftliche Arbeiten der Fachrichtung*, no. 137, pp. 130–131, 1985, leibniz Universität Hannover.

[35] J. P. Snyder, "Map projections: A working manual," US Geological Survey, Professional Paper 1395, 1987, available from http://onlinepubs.er.usgs.gov/djvu/PP/PP_1395.pdf.